01

Effect of radiation trapping on the X-ray emission spectra of multiply charged iron ions formed by ultrarelativistic laser pulses on thin foils

© M.A. Alkhimova, I.Yu. Skobelev

Joint Institute for High Temperatures of the Russian Academy of Sciences (JIHT RAS), Moscow, Russia

e-mail: maryalkhimova@ihed.ras.ru

Received March 20, 2025
Revised April 30, 2025
Accepted July 08, 2025

This paper presents the results of atom-kinetic calculations showing a significant influence of self-absorption effects on the X-ray emission spectra of plasmas formed by irradiation of thin iron foils with ultra-relativistic laser pulses. Using the spectra of hydrogen-like and helium-like iron ions as an example, it is shown that during two-pulse irradiation of the target, the relative macroscopic motion of different regions of the laser plasma with respect to each other leads to an asymmetry of the contours and a significant change in the intensity ratios of the spectral components, but can compensate for the self-absorption effects associated with the heating of the pre-plasma.

Keywords: X-ray spectroscopy, high-temperature laser plasma, X-ray spectra, self-absorption effect, multiply charged ions.

DOI: 10.61011/EOS.2025.08.62016.7708-25

Introduction

The effects of radiation trapping are one of the most important factors shaping the spectrum of line radiation in plasma. The role of these effects is primarily determined by the optical thickness τ_0 at the center of the spectral line and the electron density of the plasma. Since the absorption coefficient decreases with decreasing radiation wavelength, plasma from various sources is generally optically thick for visible and UV spectral lines and even optically thin for X-ray radiation, despite their relatively large sizes. In the case of laser plasma, characterized by high and ultrahigh densities, the plasma can be optically thick even in the X-ray range, despite its microscopic dimensions.

However, in some cases, the macroscopical movement of plasma regions relative to each other can greatly reduce the role of self-absorption in forming the emission line spectra. Even with small relative velocities V_0 the absorption coefficient at the center of the emission line, produced by one plasma region, will be proportional to $f\left(\omega_0(1+V_0/c)\right)$, which is less (and possibly significantly less) than $f(\omega_0)$. When V_0 is large, the absorption contour $f\left(\omega_0(1+V_0/c)\right)$ may no longer overlap with the emission contour $f(\omega_0)$ (which happens when $\omega_0 V_0/c \gg \Delta\omega_0$, where $\Delta\omega_0$ — the intrinsic width of the spectral line), and the plasma can become optically thin. This plasma clearing effect must always be considered when interpreting the emission spectra of laser plasma, where there is almost always relative movement between its various spatial regions, and the plasma is typically highly inhomogeneous.

The two-pulse irradiation regime of a solid foil with ultra-relativistic laser pulses of intensity greater than 10^{21} W/cm^2 is actively used in experiments aiming to create plasmas with significantly different densities. The simplest way is to delay one laser pulse relative to the other. The plasma created by the first pulse will have expanded by the time the second pulse arrives, and depending on the delay, its density may be substantially lower than that of the second plasma. The plasma created by the first pulse is called the preplasma, and the first pulse is called the pre-pulse. These laser pulses can irradiate the target from both sides or just one. If from both sides, two different laser pulses are used; if from one side, the role of the second pulse is played by its pre-pulse (or pedestal). Schemes of plasma movement formed during one-sided and two-sided irradiation are shown in Fig. 1.

From Fig. 1, it is evident that in the two-pulse regime, two plasmas moving with a relative speed of $\mathbf{V}_0$ are formed on the foil target. Under one-sided irradiation, the relative plasma movement speed can be estimated as $\mathbf{V_0} = |\mathbf{V_1} - \mathbf{V_2}|$while in the two-sided case, it is $\mathbf{V_0} = |\mathbf{V_1} + \mathbf{V_2}|$. Since the relative speed of plasma movement is considerably lower in the first case than in the second, effects of self-absorption are expected to be much less in the second case, i.e., during two-sided irradiation.

The two-sided irradiation mode has been used in experiments of collisionless acceleration of ion beams via dissipative electrostatic shock waves [1,2]. In these experiments, the first laser pulse with intensity $\sim 10^{15}$ W/cm^2 hit the back surface of the target, and then after $1-2$ ns the main pulse with intensity $\sim 10^{21}$ W/cm^2 was focused on the front surface of the target. The one-sided two-pulse irradiation occurs almost always when using pulses with picosecond and femtosecond durations possessing a natural pre-pulse unless specific measures are taken to improve the laser contrast, such as using plasma mirrors [3–5]. From a macroscopical movement perspective, the case

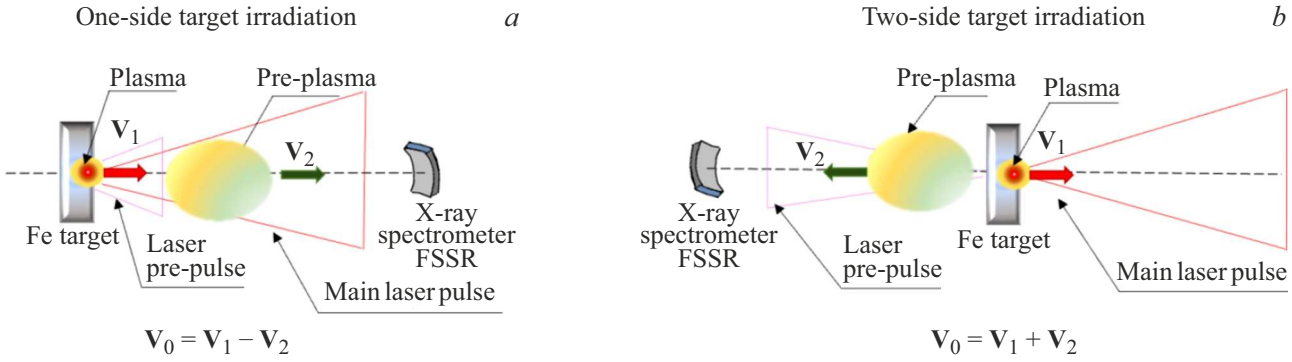

Figure 1. Scheme of the relative motion of two plasma regions with velocity $\mathbf{V}_0$ under one-sided (a) and two-sided (b) irradiation of the target-foil.

of a „controlled" pre-pulse, formed separately with a delay ranging from 500 fs to 1–2 ns before the main pulse with an intensity of at least 1% of the main laser pulse is meaningful [6–8] Thus, if the main laser pulse has an intensity on the target of about $10^{17}-10^{21}$ W/cm^2 then the pre-pulse will have an intensity of roughly $10^{15}-10^{19}$ W/cm^{2}on the target. Such a pre-pulse on iron foil can generate plasma with a temperature of several hundred electron volts and a density ranging from very low values, less than the critical electron density $N_{cr} \sim 10^{21}$ cm^{-3}, to solid ion densities $N_{solid} \sim 8 \cdot 10^{22}$ cm^{-3}.

This work presents atomic-kinetic calculations showing that radiation absorption effects, occurring during two-pulse irradiation of planar iron (Fe, atomic number $Z = 26$) foils, can lead to significant changes in the contours of observable spectral lines and to the clearing of pre-plasma. Calculations are specifically performed for the iron K-shell X-ray emission spectrum, containing lines in the wavelength range $\Delta\lambda = 1.7-1.95$ Å, corresponding to transitions in hydrogen-like FeXXVI and helium-like FeXXV ions.

Calculation results

The calculations, performed using the radiation-hydrodynamic code PrismSPECT [9], are based on the following assumptions.

Ion concentration calculations of iron were conducted within a non-stationary kinetic model described by the system of equations:

$$\frac{dN_i^Z}{dt} = \sum_{i',Z'} K_{ii'}^{ZZ'} N_{i'}^{Z'}, \qquad (1)$$

where N_i^Z is the population of the i-th level in the ion with spectroscopic symbol Z, $K_{ii'}^{ZZ'}$ is the kinetic matrix whose non-diagonal elements represent transition probabilities between states $i'Z'$ and iZ due to all elementary interactions, and the diagonal elements equal the sum of transition probabilities from state iZ to all others.

This system must be supplemented with the plasma quasi-neutrality equation:

$$\sum_{iZ} (Z-1) N_i^Z(t) = N_e(t), \qquad (2)$$

and consider the conservation law for heavy particles:

$$V(t) \sum_{iZ} N_i^Z(t) = N_0 V_0, \qquad (3)$$

where N_0 is the initial concentration of atoms in the target,V_0 is the initial plasma volume, and $N_e(t)$ and $V(t)$ are the electron concentration and plasma volume at time t.

The elements of the kinetic matrix depend on plasma parameters, i.e., temperature and free electron concentration. These parameters enter the probabilities of collisional transitions. If the plasma parameters do not change over time, then at $t \to \infty$ the level populations tend toward their stationary values (which, however, can be thermodynamically non-equilibrium), which can be determined from the system of stationary kinetic equations.

The kinetic matrix$K_{ii'}^{ZZ'}$ contains the probabilities of all elementary processes occurring in the plasma. Since, for the highly charged ions of interest to us, the probabilities of multi-electron ionization are significantly lower than those of single-electron ionization, it can be assumed that the kinetic matrix elements are nonzero only in cases where $(Z - Z') = 0, \pm 1$. The kinetic matrix element corresponding to $(Z - Z') = 0$can be represented as the sum of probabilities of spontaneous radiative transition, stimulated radiative transitions, and collisional transitions. If $(Z - Z') = 1$, then the kinetic matrix elements equal the sum of probabilities of autoionization, photoionization, and collisional ionization. Finally, in the case of $(Z - Z') = -1$ the kinetic matrix elements equal the sum of probabilities of collisional (three-body) recombination, photorecombination, and dielectronic capture. All the above elementary processes were considered in solving the kinetic system.

First, let's consider the case of single-pulse heating, when dense, high-temperature plasma is formed by irradiating an iron foil target of thickness $1-5\,\mu$m with a high-contrast laser pulse of ultrarelativistic intensity. The radiation

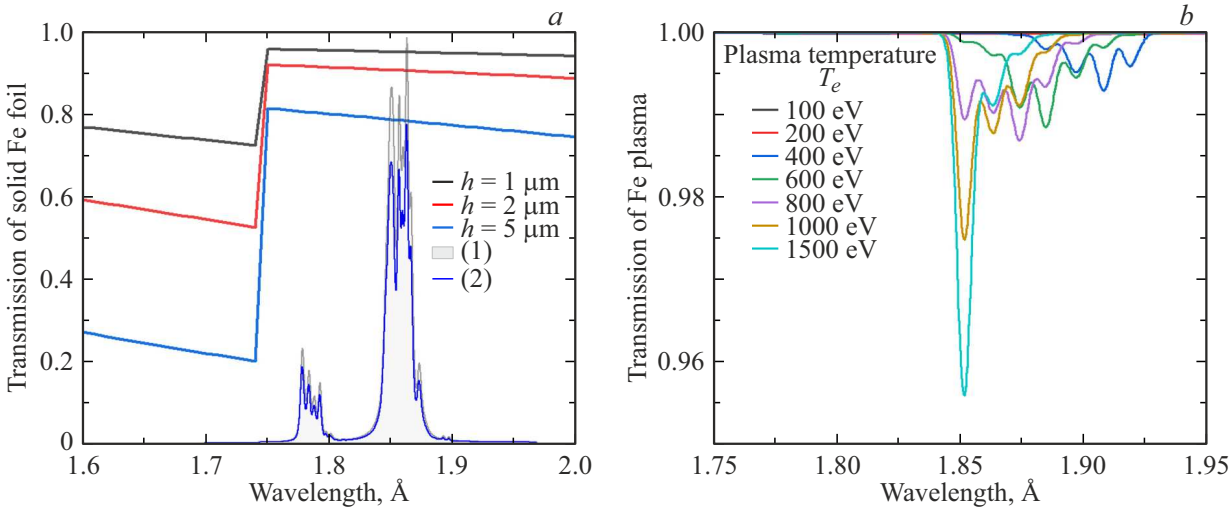

Figure 2. (*a*) Model spectrum of iron plasma calculated using PrismSPECT, and transmission curves of X-ray radiation through solid iron foil with thickness $h = 1, 2, 5\,\mu$m, calculated in [12]. (*b*) Calculation of the plasma transmission function with critical electron density $N_e = N_{\rm cr} = 10^{21}\,{\rm cm}^{-3}$ and thickness $l_p = 2\,\mu$m depending on the plasma electron temperature T_e.

spectrum of such plasma contains lines corresponding to transitions in the hydrogen-like iron ion Fe,XXVI and lines corresponding to transitions in the helium-like ion Fe,XXV. Such spectra have been repeatedly observed in experiments on sub-PW power laser facilities [10–12]. A typical emission spectrum of such plasma, calculated using the radiation-collisional code PrismSPECT [9] for a flat plasma layer with a thickness of $l_p = 0.5\,\mu$m, electron temperature $T_e = 1800$ eV and solid ion density $N_i = N_{\rm solid} = 8 \cdot 10^{22}\,{\rm cm}^{-3}$, is shown in Fig. 2, *a*. Also shown are the transmission curves of X-ray radiation by solid iron foil of thickness $1-5\,\mu$m, calculated in [13].

The initial model Fe plasma spectrum (highlighted in light gray and marked with index (1)) (in Fig. 2, *a* contains the resonance doublet $\mathrm{Ly}_{\alpha 1,2}$ (wavelengths 1.77, 1.78 Å) of hydrogen-like FeXXVI ion with corresponding dielectronic satellites, and the resonance and intercombination lines $\mathrm{He}_{\alpha 1,2}$ (wavelengths 1.85, 1.86 Å) of helium-like FeXXV ion with Li-, Be-, and B-like satellites. If the spectrometer observes the rear side of the target, as seen in Fig. 2, *a*, the original spectrum is somewhat absorbed in the cold part of the target, but for foil thicknesses up to $5\,\mu$m inclusive (blue curve in Fig. 2, *a*) the changes in line contours and relative component intensity are very minor. For thicker foils, absorption becomes significant and must be taken into account [14].

Now consider the case of two-pulse irradiation. The first pulse, regardless of whether it is focused on the front or rear surface, will be called the pre-pulse, and the plasma it creates is called preplasma. Depending on the delay between the pulses, the preplasma density at the time the main plasma forms may remain close to solid or decrease substantially. Suppose the pre-pulse creates plasma with critical electron density $N_e = N_{\rm cr} = 10^{21}\,{\rm cm}^{-3}$ and thickness $l_p = 2\,\mu$m. Fig 2., *b*shows the calculated transmission of such preplasma depending on its electron temperature T_e. It is seen that even at $T_e = 1500$ eV preplasma at critical density remains transparent to X-rays in the studied wavelength range 1.7–1.95 Å (photon energies 6–7 keV) and no absorption effects are observed.

A different picture appears at small delays when the preplasma has no time to expand and has nearly solid density by the arrival of the main pulse. Fig. 3 shows transmission functions of the preplasma with density $N_i = N_{\rm solid} = 8 \cdot 10^{22}\,{\rm cm}^{-3}$ as a function of electron temperature T_e for various plasma layer thicknesses l_p. It is clear from Fig. 3 that transmission of dense preplasma strongly depends on both the plasma temperature and thickness. Even at a small preplasma thickness $\sim 0.5\,\mu$m and temperature 400 eV, intense absorption of lines in the wavelength range 1.87–1.92 Å, occurs; increasing temperature to 800 eV shifts the absorption region toward shorter wavelengths and includes the region near 1.85 Å, which contains lines He_α. From Fig. 3, *b* it is evident that increasing plasma layer thickness enhances absorption. At a thickness of $1\,\mu$m absorption of 80–100% of radiation in the 1.85–1.90 Å range occurs at $T_e \geq 600$ eV (Fig. 3, *b*).

Fig. 4 shows how the original iron plasma spectrum changes after passing through preplasma of thickness $l_p = 0.5\,\mu$m, if its temperature varies from 400 to 800 eV. The temperature of plasma formed by the pre-pulse noticeably influences the spectrum appearance: at 400 eV, changes occur in the intensity ratio of the $\mathrm{He}_{\alpha 1,2}$ lines and decrease in the satellite group intensity to He_α(red curve in Fig. 4). Increasing preplasma temperature to 800 eV leads to maximal absorption in the He_α region, while the spectrum around the Ly_αline and its He-like satellites remains unchanged.

So far, the relative motion of preplasma and plasma has not been taken into account. However, the absorp-

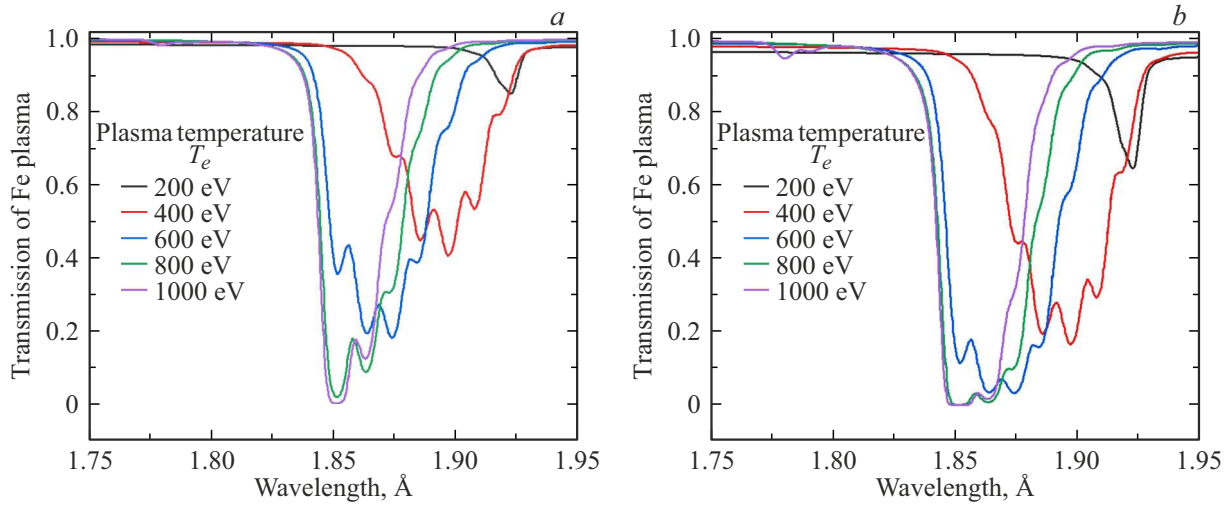

Figure 3. Dependence of the transmission function of iron preplasma with solid density $N_i = N_{\text{solid}} = 8 \cdot 10^{22}\,\text{cm}^{-3}$ on electron temperature at various preplasma thicknesses: $l_p = 0.5$ (a), $1\,\mu$m (b).

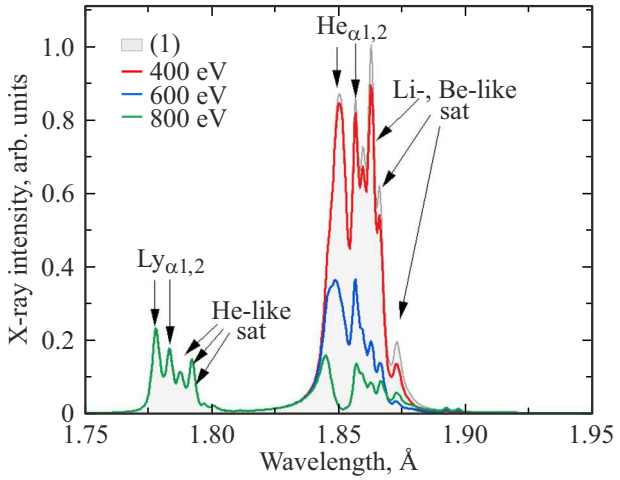

Figure 4. Calculation of transmission of the original iron plasma emission spectrum (gray curve), calculated for $T_e = 1800\,\text{eV}$, $N_i = N_{\text{solid}} = 8 \cdot 10^{22}\,\text{cm}^{-3}$, $l_p = 0.5\,\mu$m, passing through colder solid preplasma of thickness $l_p = 0.5\,\mu$m at electron temperatures 400, 600, 800 eV.

tion behavior becomes more complex when this effect is considered. Let V_0 be the relative macroscopic velocity between the two plasma regions, with a characteristic value $\sim 10^7 - 10^8$ cm/s [15]. Then the emission and absorption spectra will be shifted relative to each other by $\lambda(V_0/c)$.

We use the reference frame associated with the emitting plasma. In the case of two-sided heating (Fig. 1, b) $V_0 = V_1 + V_2$ and the absorption spectrum shifts toward shorter wavelengths. Fig. 5 upper panels show transmission functions of solid iron plasma at temperatures 400 (Fig. 5, a), 600 (Fig. 5, b), and 800 eV (Fig. 5, c) calculated for various relative velocities V_0. The lower panels demonstrate the changes of the original spectrum caused by passage through preplasma moving relative to the emitting plasma. From Fig. 5 it follows that at relative velocity $V_0 \sim 10^6 - 10^7$ cm/s the absorption spectrum shift is a few hundredths of an angstrom, much less than the characteristic width of the emitted lines. In this case, the relative velocity effect barely influences observed emission spectra. As V_0 increases, absorption of the resonance line $He_{\alpha 1}$ intensifies and absorption of longer-wavelength dielectronic satellites associated with Li-, Be-, B-like ions decreases. Fig. 5 shows that at $V_0 \geq 10^8$ cm/s the absorption region noticeably shifts toward shorter wavelengths, leading at $T_e \sim 600 - 800$ eV to increased intensity of $He_{\alpha 1,2}$lines. From Fig. 5, c it is seen that at $T_e = 800$ eV and $V_0 \sim 7 \cdot 10^8$ cm/s absorption effects practically disappear for the He_α line and its satellites, with no absorption effects in the Ly_αregion.

In the case of one-sided heating (Fig. 1, a) $V_0 = V_1 - V_2$, and the absorption spectrum shifts toward longer wavelengths. Results for this case are shown in Fig. 6, where upper panels show transmission functions of solid iron plasma at temperatures 400 (Fig. 6, a), 600 (Fig. 6, b), and 800 eV (Fig. 6, c), for different relative velocities V_0 and the lower panels show the changes in the original spectrum caused by passage through preplasma. Fig. 6 shows that at $T_e \sim 400$ eV the redshift of the absorption region results in preplasma transparency within $\Delta\lambda = 1.7 - 1.87$ Å and the original emission spectrum changes little. The subsequent increase in temperature leads to a short-wavelength shift of the absorption region by an average of 0.03 Åfor every 200 eV, which cannot be compensated by a long-wavelength shift due to the relative motion of the plasma at speeds of $V_0 \sim 10^6 - 10^8$ cm/s. This leads to significant absorption of the spectrum region $\Delta\lambda = 1.84 - 1.90$ Å, containing $He_{\alpha 1,2}$ lines and satellites. Figs. 6, b, c show that at $V_0 > 10^8$ cm/s the absorption region noticeably shifts toward longer wavelengths, increasing the intensity of $T_e \sim 600 - 800$ eV lines at $He_{\alpha 1,2}$ and restoring the profile of Li-, Be-like

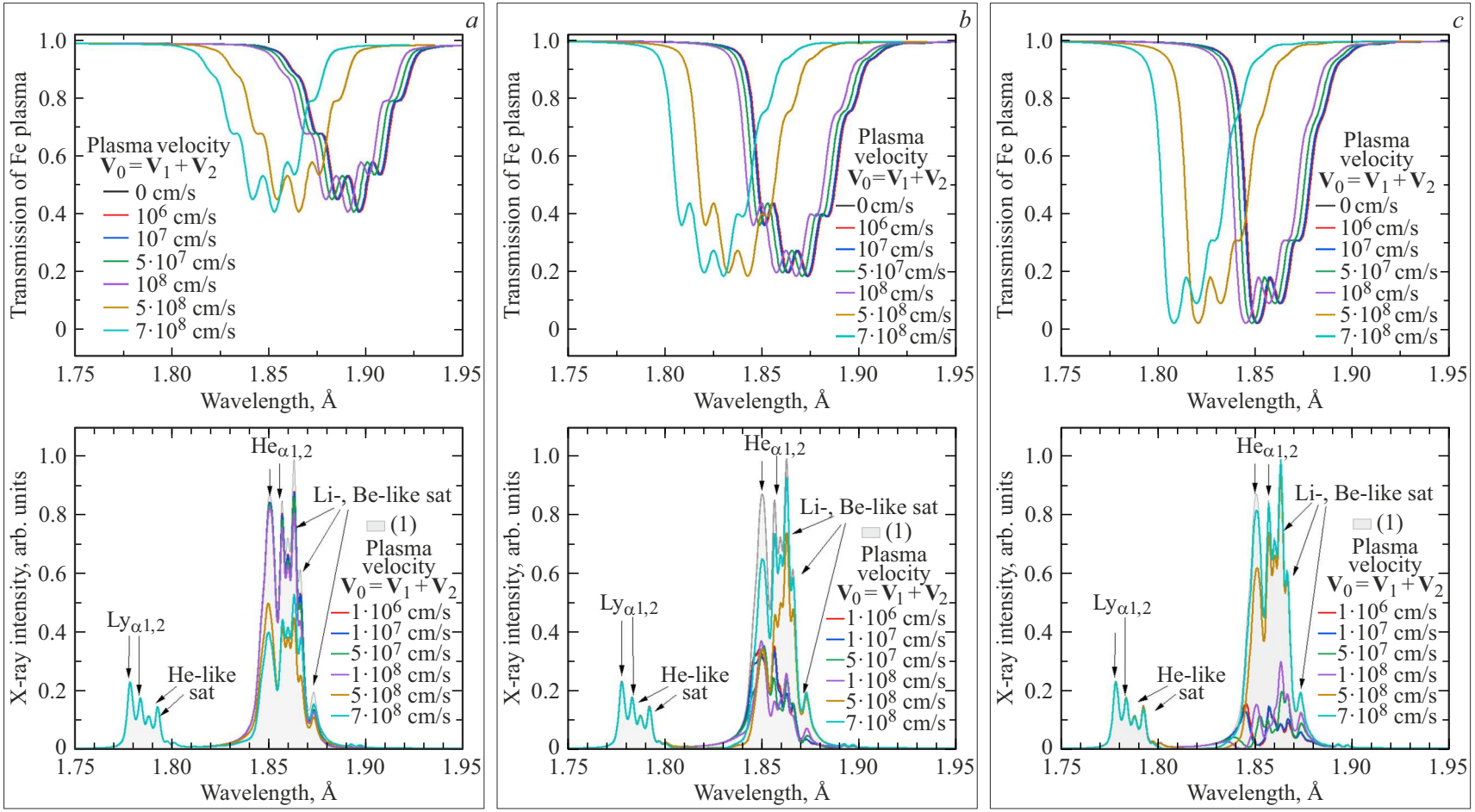

Figure 5. Transmission functions of solid iron plasma at temperatures 400 (*a*), 600 (*b*), and 800 eV (*c*), calculated for various relative velocities $V_0 = |\mathbf{V}_1 + \mathbf{V}_2|$ (upper panels); original spectrum passing through moving preplasma (lower panels).

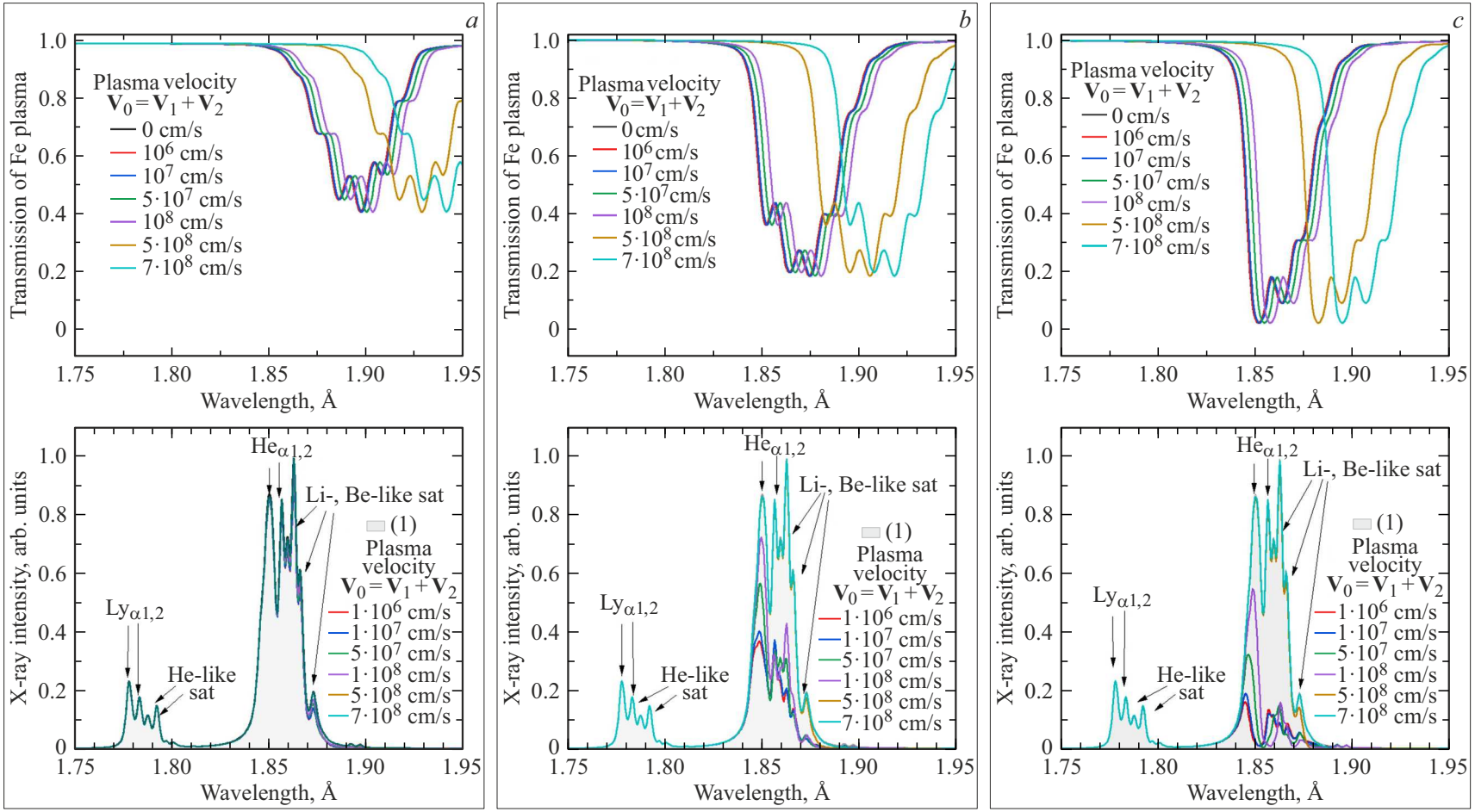

Figure 6. Transmission functions of solid iron plasma at temperatures 400 (*a*), 600 (*b*), and 800 eV (*c*), calculated for various relative velocities $V_0 = |\mathbf{V}_1 + \mathbf{V}_2|$ (upper panels); original spectrum passing through moving preplasma (lower panels).

satellite groups. At $V_0 \sim 7 \cdot 10^8$ cm/s absorption effects are practically absent for $He_{\alpha 1,2}$line and satellites.

Conclusion

The calculations presented in this study for X-ray K-emission spectra of plasma in thin iron foils confirm that radiation trapping effects always occur in the two-pulse irradiation regime of targets, both for one-sided and two-sided heating. The formation of preplasma, depending on its density, temperature, and expansion velocity, can significantly influence the configuration of the X-ray emission spectrum and can change the intensity ratio of spectral components by several times. While absorption effects of photons with energies of $6-7$ keV are negligible in cold foil targets with thickness up to $5\,\mu$m, their influence can become significant during heating even with relatively thin preplasma layers $\sim 1\,\mu$m. Increasing preplasma temperature shifts the absorption region toward the short-wavelength part of the spectrum, creating transparency windows for spectral components in the longer-wavelength region.

It should be noted that preplasma that is both very dense and quickly moving will strongly affect the nature of absorption. Simultaneous fulfillment of both conditions apparently occurs only either with a significant sub-picosecond pre-pulse accompanying the main laser pulse or with nearly synchronous (sub-picosecond delay) multi-beam irradiation. If the delay is substantially longer (subnanosecond or even nanosecond), the density of the absorbing preplasma, and therefore its absorption coefficient at the moment of main pulse arrival, will become much lower. However, if quasi-one-dimensional expansion of preplasma is ensured due to a large diameter of the pre-pulse focal spot, the decrease in absorption coefficient can be largely compensated by the increased preplasma thickness, making absorption (and clearing) effects important in this case as well.

The results of the present work imply that analysis of spectral data obtained in modern experiments on laser facilities with power around $1-10$ PW, must include possible absorption of emission spectra by moving preplasma, since already at laser pulse intensities $\sim 0.3-0.5$ PW plasma velocities reach 10^8 cm/s [16]. Note that radiation trapping effects can be especially important in multi-beam laser irradiation scenarios of targets with various geometries, where many plasma regions move relative to each other.

Funding

The study was supported by the Ministry of Science and Higher Education of the Russian Federation (State Assignment No. 075-00269-25-00).

Conflict of interest

The authors declare that they have no conflict of interest.

References

[1] W. Zhang, H. Cai, S. Zhu. Plasma Phys. Control. Fusion., **60**, 055001 (2018). DOI: 10.1088/1361-6587/aab175

[2] R. Kumar, Y. Sakawa, L.N.K. Döhl, N. Woolsey, A. Morace. Phys. Rev. Accel. Beams., **22**, 043401 (2019). DOI: 10.1103/PhysRevAccelBeams.22.043401

[3] A. Kon, M. Nishiuchi, Y. Fukuda, K. Kondo, K. Ogura, A. Sagisaka, Y. Miyasaka, N.P. Dover, M. Kando, A.S. Pirozhkov, I. Daito, L. Chang, I.W. Choi, C.H. Nam, T. Ziegler, H.-P. Schlenvoigt, K. Zeil, U. Schramm, H. Kiriyama. High Power Laser Sci. Eng., **10**, e25 (2022). DOI: 10.1017/hpl.2022.15

[4] C. Thaury, F. Quéré, J.-P. Geindre, A. Levy, T. Ceccotti, P. Monot, M. Bougeard, F. Réau, P. D'Oliveira, P. Audebert, R. Marjoribanks, P. Martin. Nat. Phys., **3**, 424–429 (2007). DOI: 10.1038/nphys595

[5] G. Doumy, F. Quéré, O. Gobert, M. Perdrix, P. Martin, P. Audebert, J.C. Gauthier, J.-P. Geindre, T. Wittmann. Phys. Rev. E., **69**, 026402 (2004). DOI: 10.1103/PhysRevE.69.026402

[6] U. Teubner, P. Gibbon, Rev. Mod. Phys., **81**, 445–479 (2009). DOI: 10.1103/RevModPhys.81.445

[7] T. Nakamura, J.K. Koga, T.Z. Esirkepov, M. Kando, G. Korn, S.V. Bulanov. Phys. Rev. Lett., **108**, 195001 (2012). DOI: 10.1103/PhysRevLett.108.195001

[8] Y. Hanada, K. Sugioka, I. Miyamoto, K. Midorikawa. Appl. Surf. Sci., **248**, 276–280 (2005). DOI: 10.1016/j.apsusc.2005.03.050

[9] PrismSPECT. [Electronic source]. URL: https://prism-cs.com/Software/PrismSPECT/overview.html

[10] A. Stafford, A.S. Safronova, A.Y. Faenov, T.A. Pikuz, R. Kodama, V.L. Kantsyrev, I. Shrestha, V.V. Shlyaptseva. Laser Part. Beams., **35**, 92–99 (2017). DOI: 10.1017/S026303461600077X

[11] M.A. Alkhimova, A.Y. Faenov, I.Y. Skobelev, T.A. Pikuz, M. Nishiuchi, H. Sakaki, A.S. Pirozhkov, A. Sagisaka, N.P. Dover, K. Kondo, K. Ogura, Y. Fukuda, H. Kiriyama, K. Nishitani, T. Miyahara, Y. Watanabe, S.A. Pikuz, M. Kando, R. Kodama, K. Kondo. Opt. Express. **25**, 29501 (2017). DOI: 10.1364/OE.25.029501

[12] M.A. Alkhimova, A.Y. Faenov, T.A. Pikuz, I.Y. Skobelev, S.A. Pikuz, M. Nishiuchi, H. Sakaki, A.S. Pirozhkov, S. Sagisaka, N.P. Dover, K. Kondo, K. Ogura, Y. Fukuda, H. Kiriyama, T. Esirkepov, S.V. Bulanov, A. Andreev, M. Kando, A. Zhidkov, K. Nishitani, T. Miyahara, Y. Watanabe, R. Kodama, K. Kondo. J. Phys. Conf. Ser., **946**, 012018 (2018). DOI: 10.1088/1742-6596/946/1/012018

[13] B.L. Henke, E.M. Gullikson, J.C. Davis. At. Data Nucl. Data Tables., **54**, 181–342 (1993). DOI: 10.1006/adnd.1993.1013

[14] A.S. Martynenko, S.A. Pikuz, I.Y. Skobelev, S.N. Ryazantsev, C.D. Baird, N. Booth, L.N.K. Döhl, P. Durey, A.Y. Faenov, D. Farley, R. Kodama, K. Lancaster, P. McKenna, C.D. Murphy, C. Spindloe, T.A. Pikuz, N. Woolsey. Matter Radiat. Extrem., **6**, 014405 (2021). DOI: 10.1063/5.0025646

[15] R. Zemskov, K. Burdonov, A. Soloviev, A. Sladkov, A. Korzhimanov, J. Fuchs, D. Bisikalo, A. Zhilkin, M. Barkov, A. Ciardi, W. Yao, M. Glyavin, M. Morozkin, M. Proyavin, A. Luchinin, P. Chuvakin, V. Ginzburg, A. Kochetkov, A. Kuzmin, A. Shaykin, I. Shaikin, S. Perevalov, A. Kotov, S. Pikuz, S. Ryazantsev, E. Khazanov, M. Starodubtsev. Astron. Astrophys., **681**, A37 (2024). DOI: 10.1051/0004-6361/20224525

[16] N.L. Kugland, D.D. Ryutov, P.-Y. Chang, R.P. Drake, G. Fiksel, D.H. Froula, S.H. Glenzer, G. Gregori, M. Grosskopf, M. Koenig, Y. Kuramitsu, C. Kuranz, M.C. Levy, E. Liang, J. Meinecke, F. Miniati, T. Morita, A. Pelka, C. Plechaty, R. Presura, A. Ravasio, B.A. Remington, B. Reville, J.S. Ross, Y. Sakawa, A. Spitkovsky, H. Takabe, H.-S. Park. Nat. Phys., **8**, 809–812 (2012). DOI: 10.1038/nphys2434

Translated by J.Savelyeva